
Contrasting Intra-Modal and Ranking Cross-Modal Hard Negatives to Enhance Visio-Linguistic Fine-grained Understanding

Le Zhang Rabiul Awal Aishwarya Agrawal
Mila - Quebec AI Institute
Université de Montréal
{le.zhang, aishwarya.agrawal}@mila.quebec

Abstract

Current Vision and Language Models (VLMs) demonstrate strong performance across various vision-language tasks, yet they struggle with fine-grained understanding. This issue stems from weak image-caption alignment in pretraining datasets and a simplified contrastive objective that fails to distinguish nuanced grounding elements such as relations, actions, and attributes. As a result, the models tend to learn bag-of-words representations. To mitigate these challenges, we introduce an intra-modal contrastive loss and a unique cross-modal rank loss with an adaptive threshold that serves as curriculum learning, utilizing our automatically generated hard negatives to augment the model’s capacity. Our strategy, which does not necessitate additional annotations or parameters, can be incorporated into any VLM trained with an image-text contrastive loss. Upon application to CLIP, our method leads to significant improvements on three fine-grained benchmarks, and it also enhances the performance of X-VLM, which is the state-of-art model on fine-grained reasoning.¹

1 Introduction

The vision-language research field has witnessed significant advancements over recent years, driven by the emergence of web-scale datasets [25, 5], transformer-based model architectures, and innovative training objectives like contrastive learning. Contemporary vision-language models (VLMs) have even demonstrated the capacity to exceed human performance in certain tasks, such as Visual Question Answering (VQA) [7]. They have also shown promising capabilities in zero-shot generalization to previously unseen tasks or datasets, including zero-shot VQA, captioning [13, 18, 1], and zero-shot image-retrieval on unseen datasets [23, 35, 28]. Despite these remarkable strides, current models still exhibit deficiencies in comprehending fine-grained details of relations, attributes, objects and actions [34, 29]. For example, they struggle to accurately interpret phrases like "Horse is eating the grass" versus "Grass is eating the horse" [34] when presented with a corresponding image. We contend that such nuanced understanding is pivotal for further advancements in vision-language research.

A primary factor impeding fine-grained understanding in current models stems from their training methodology. These models are trained on web-scale image-text pairs using objectives like image-text contrastive (ITC) loss [23]. This strategy optimizes the model to differentiate between correct image-text pairs and a vast array of incorrect ones. However, the incorrect pairs are often markedly distinct, and the model can distinguish them primarily through object recognition, without needing to grasp fine-grained details such as attributes and relations. Fig 2 illustrates an example of fine-grained relational understanding.

¹Code is available <https://github.com/Magiccircuit/Enhance-FineGrained>

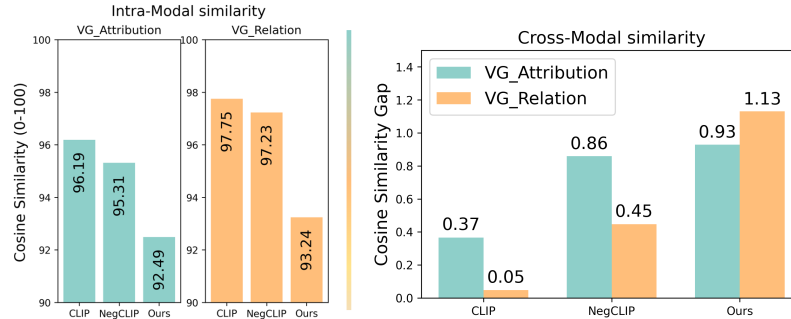


Figure 1: (Left) Existing methods (CLIP and NegCLIP) demonstrate high intra-modal similarity between positive and hard negative captions which is not desirable, while our method shows reduced similarity. The similarity measure we use is cosine similarity which is a normalized inner product between the two caption embeddings obtained from the model. (Right) Existing methods also show small gap between true and hard negative cross-modal (image-caption) similarity, while our method increases this gap.

To address this shortcoming, prior work such as NegCLIP [34] has utilized phrase parsing and swapping to generate captions that exhibit structural similarities but differ semantically. By incorporating these captions as additional negatives within the ITC loss, the performance of the CLIP model is considerably enhanced. However, this method is not without its limitations. An analysis of the intra-modal similarity between positive and hard negative captions for the CLIP and NegCLIP models, illustrated in Fig 1 (Left), indicates that for these models, captions with similar structure but different meanings (hard negatives) possess highly similar representations. We hypothesize that a larger similarity gap between true and hard negative captions would foster improved fine-grained understanding. Furthermore, as indicated in Fig 1 (Right), the gap between correct image-text pair similarity and hard negative pair similarity is minimal. These observations suggest that the model may not be fully comprehending the intricacies of intra-modality and cross-modality semantics.

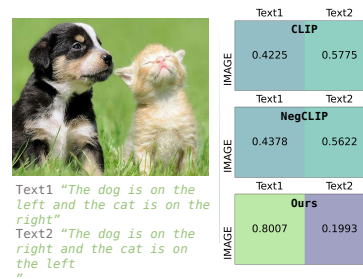


Figure 2: (Left) Relation understanding Example. (Right) Image-Text similarity for three models.

In response to these challenges, we propose a rule-based methodology for generating similar-sounding captions that specifically target varied aspects like relations, attributes, actions, and objects. Additionally, we introduce two supplementary losses: (1) the intra-modality contrastive loss, devised to stimulate the model to differentiate semantic nuances within a single modality, and (2) the cross-modality rank loss, designed to guide the model to maintain a minimum distance between true image-text pair and the hard negative image-text pairs. Furthermore, this minimum distance (or threshold) is adaptive in nature, i.e., its value is adaptively determined based on the model’s ability to discriminate between positives and hard negatives. As training progresses and the model’s performance improves, the threshold increases correspondingly, signifying the rising difficulty of the problem and the model’s enhanced capability, thereby embodying a curriculum learning approach. We apply these losses to two representative models, namely, the widely-used CLIP² and top-performing fine-grained X-VLM[35]. Upon evaluation across various datasets, our method enhances both the X-VLM and CLIP models. Specifically, when applied to CLIP, it achieves an improvement of 23.7% and 13.5% respectively in the Relation and Attribution splits of the ARO benchmark [34] compared to the baseline, surpassing the state-of-the-art NegCLIP by 2.8% and 5.9%. On the VALSE dataset, our approach improves the baseline by an average of 7.2% and outperforms NegCLIP by 0.9%. On the VL-CheckList, our method increases the baseline performance by 5.9%, exceeding NegCLIP by an average of 1.7%. When applied to X-VLM, it improves 0.5% and 2.5% on ARO-Relation and ARO-Attribution, 1.3% on VALSE and 2.1% on VL-CheckList compared with coco fine-tuned checkpoint.

²Given that our method is grounded in ITC, it is generalizable and can be applied to any models incorporating an ITC loss

To summarize, the main contributions of this article are: (1) We devise a method for generating hard negatives that overcomes the existing limitations in ITC loss. This method incorporates a variety of negatives based on distinctive features. (2) We introduce an intra-modal contrastive loss that leverages the generated hard negatives to tackle the challenge of high text similarity in VLMs. (3) We propose a cross-modal rank loss with threshold, encouraging the model to maintain a disparity between cross-modal positive and hard negative similarities, and (4) We make the threshold to be adaptive, acting as a form of curriculum learning that adjusts to the model’s evolving capability. (5) We establish enhanced performance on multiple benchmarks using our proposed losses. This assertion is supported by extensive experiments and ablation studies, which illuminate the efficacy and design of our approach.

2 Related Work

Vision-language Models VLMs such as CLIP [23], ALIGN [11], X-VLM [35], COCA[33], FLAVA[26] typically encompass a text encoder and an image encoder. These models are trained on extensive, noise-rich multimodal datasets utilizing a combination of loss functions like Grounded (Masked) Language Modeling, Masked Image Modeling, Image Text Matching, and Image Text Contrastive Learning. The Image Text Contrastive (ITC) loss [23] is the most common, as it strives to minimize the distance between aligned image-text pairs and maximize the distance between unaligned pairs. These unaligned pairs, also known as negatives, are randomly sampled within the batch. Due to the large-scale pretraining datasets, VLMs have demonstrated exceptional zero-shot performance across diverse visual-language tasks [23, 11, 26]. However, recent research indicates that these models often learn a "bag of words" representation [4, 34], limiting their fine-grained understanding.

Visio-linguistic fine-grained understanding evaluation Several benchmarks have been recently introduced to assess the fine-grained understanding of VLMs, concentrating on aspects like relations, attributes, objects, and more. For instance, ARO[34] emphasizes understanding of attributes and relations, VL-checklist[36] targets finer subcategories such as size, color, action, and spatial relations. VALSE[21] focuses on linguistic phenomena including existence, counting, plurality, and coreference, while Winoground[29] and CREPE[16] concentrate on compositional understanding and complex reasoning, encompassing commonsense and external knowledge. These benchmarks are designed as cross-modal retrieval tasks, where the goal is to distinguish between correct and incorrect captions given an image, evaluated on accuracy.

Approaches for enhancing visio-linguistic fine-grained understanding Recent papers[34, 4, 19] have pointed out that the popular ITC loss used to train VLMs is not sufficient to learn fine-grained understanding as the positives and negatives do not have fine-grained differences. It’s easy for the model to achieve low loss by just paying attention to objects existence. And hence these methods propose generating hard-negatives and fine-tuning the pretrained models with hard-negatives. For instance, NegCLIP [34] incorporates this concept by generating hard negatives through randomly swapping two phrases and utilizing them as additional negatives for the ITC. Similarly, Doveh et al. [4] generate extra captions as negatives and analogies, employing negatives for the image-text contrastive loss and analogies for an additional alignment loss. Paiss et al. [19] modify the count in captions, compelling the model to encourage the model to pay attention to different counts of objects. An alternative line of work focuses on not using hard negatives, but instead imposes a variant of ITC loss to force the model to learn fine-grained information. For example, Wang et al. [31] propose an auxiliary regularization loss for equivariant training, while Pandey et al. [20] introduce a cross-modal attention congruence regularization loss for relation alignment. More recently, several studies[9, 27] utilize additional scene graph annotations to boost structural understanding, which requires complex pre-processing. However, our method distinguishes itself by not requiring any additional annotations.

Previous studies [34, 4] have employed techniques to generate negatives through random word-swapping. In contrast, our method systematically generates a variety of *hard negatives*, each corresponding to distinct features, thereby attaining superior performance. Moreover, the losses we propose are constructed upon these diversely featured *hard negatives*, further distinguishing our approach from earlier methods. Additionally, previous studies have neglected the high similarity between hard negatives within a single modality. While all proposed losses concentrate on multimodal representation interactions, we propose a simple inner-modality contrastive loss to address this issue.

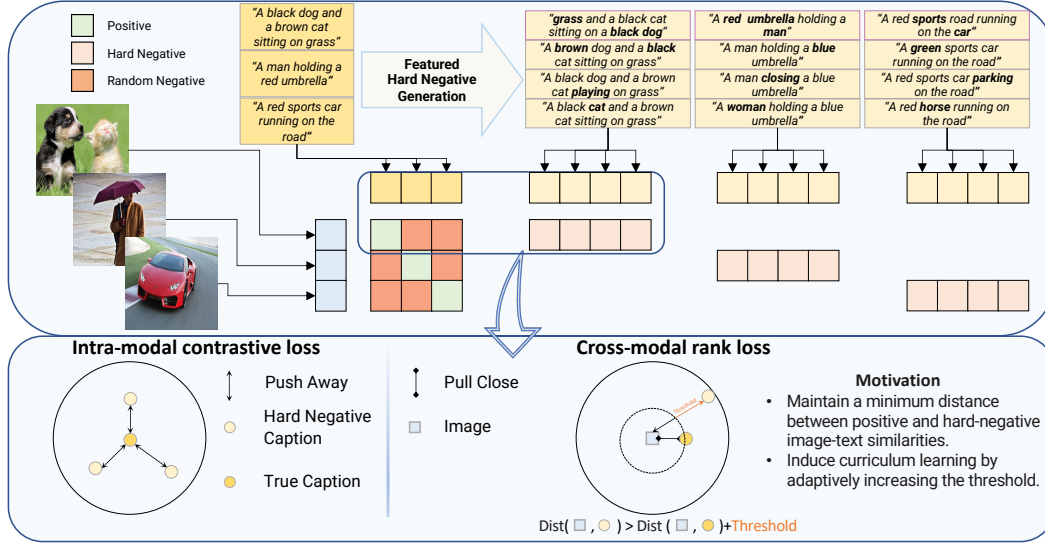


Figure 3: (Top) An overview of our method’s pipeline. (Bottom) Illustration of the two proposed loss functions.

3 Method

In the proposed method, we introduce two loss functions that are specifically applied to the automatically generated *hard negatives*. In this section, we first discuss the process of hard negative generation, followed by a detailed description of our loss functions.

3.1 Featured Hard Negative Generation

In contrastive learning, *hard negatives* refer to instances that exhibit high similarity to positive samples, yet do not qualify as positive themselves. Consider the following caption as an example: "A gray cat sits on top of a wooden chair near a plant." A potential hard negative could be: "A gray cat sits on top of a plastic chair near a plant." While the hard negative correctly identifies the majority of elements in the image, it diverges from the positive sample with regards to the chair’s material. Incorporating *hard negatives* into the training process can enable models to discern subtle distinctions, thereby enhancing their overall accuracy and performance[8, 6, 17, 22, 12, 24].

To bolster the fine-grained understanding of our model, we deliberately create *hard negatives* that embody various alterations to the original captions. These adjustments encompass changes in the relationship, attributes, and action of the image’s objects. Furthermore, we produce *hard negatives* where we replace an object name with another, encouraging the model to distinguish between different objects. To generate these *hard negatives*, we employ Part-Of-Speech (POS) parsing and Language Models. Utilizing Spacy[10], we parse the captions and assign POS tags to each word. For relational *hard negatives*, we interchange the positions of two noun words. For attribution, action, and object name alterations, we randomly mask an adjective, verb, or noun word, and subsequently fill in the masked area using the RoBERTa[15], simplified examples are shown in Fig 3. For each caption, we generate all four types of *hard negatives*, replacing any examples in which the requisite words or two objects are absent from the caption with a placeholder string. This approach ensures a comprehensive and robust training dataset for enhancing our model’s performance.

3.2 Proposed Losses

Preliminaries Most recent VLMs have a vision encoder $f_i : X_{image} \rightarrow \mathbb{R}^d$ and a text encoder $f_t : X_{text} \rightarrow \mathbb{R}^d$. The similarity between two inputs I, T using their encoders f_i, f_t are computed as: $S(I, T) = \frac{f_i(I) \cdot f_t(T)}{\|f_i(I)\| \cdot \|f_t(T)\|} / \tau$ where \cdot represents inner product and τ is a trainable temperature parameter. The image-text contrastive loss is applied on the computed similarity. Considering image-text pairs (I, T) within a batch \mathcal{B} , the computation of the Image-Text Contrastive (ITC) loss is

formulated as follows:

$$\mathcal{L}_{itc} = \sum_{(I,T) \in \mathcal{B}} - \left(\log \frac{\exp^{S(I,T)}}{\sum_{T_i \in \mathcal{B}} \exp^{S(I,T_i)}} + \log \frac{\exp^{S(I,T)}}{\sum_{I_j \in \mathcal{B}} \exp^{S(I_j,T)}} \right) \quad (1)$$

For each image-text pair (I, T) , prior research methodologies often generate a single hard negative caption T_{hn} through the random swapping of a word. This generated *hard negatives* is subsequently treated as an additional set of random negatives. Thus, the formulation of the Image-Text Contrastive (ITC) loss with the inclusion of a *hard negatives* [34] can be described as follows:

$$\mathcal{L}_{itc(hn)} = \sum_{(I,T) \in \mathcal{B}} - \left(\log \frac{\exp^{S(I,T)}}{\sum_{T_i \in \mathcal{B}} \exp^{S(I,T_i)} + \sum_{T_k \in \mathcal{T}_{hn}} \exp^{S(I,T_k)}} + \log \frac{\exp^{S(I,T)}}{\sum_{I_j \in \mathcal{B}} \exp^{S(I_j,T)}} \right) \quad (2)$$

Intra-Modal Contrastive loss Adhering to the aforementioned notations and given an image-text pair (I, T) within batch \mathcal{B} , our method, as outlined in Section 3.1, generates four distinct hard negatives $\mathcal{T}_{hn} = \{T_{rel}, T_{att}, T_{act}, T_{obj}\}$ corresponding to changes in relation, attributes, actions and object names. The primary motivation behind employing intra-modal contrastive (IMC) loss is to promote the model’s ability to discern semantic differences between true and hard-negative captions. Concurrently, it is crucial to maintain the model’s multimodal alignment capacity while contrasting single modality representations. Consequently, the formulation of this loss can be articulated as follows:

$$\mathcal{L}_{imc} = \sum_{(I,T) \in \mathcal{B}} - \log \frac{\exp^{S(I,T)}}{\sum_{T_k \in \mathcal{T}_{hn}} \exp^{S(T,T_k)}} \quad (3)$$

Cross-Modal Rank loss with adaptive threshold We aim to maintain a minimum distance between the positive and hard negative image-text pairs. This is achieved by introducing a threshold, which ensures that the similarity score of an image-text pair $S(I, T)$ exceeds the similarity score of any image and hard negative pair $S(I, T_k)$ by at least a threshold value Th_k corresponding to the type of hard-negative. This can be formally expressed as:

$$S(I, T) > \{S(I, T_k) + Th_k | T_k \in \mathcal{T}_{hn}\}$$

Inspired by the hinge loss concept, we employ this threshold in the loss function, which we call Cross-modal Rank (CMR) loss, defined as follows:

$$\mathcal{L}_{cmr} = \sum_{(I,T) \in \mathcal{B}} \sum_{T_k \in \mathcal{T}_{hn}} \max(0, S(I, T_k) - S(I, T) + Th_k) \quad (4)$$

Defining the threshold (margin) for hinge loss can be a challenging task[30]. Rather than treating the threshold as a fixed value and conducting hyperparameter search, we use an adaptive threshold which is a function of the difference in model’s similarity scores between the true pair and the *hard negatives* pair. It’s noteworthy that this difference could be viewed as a measure of the model’s fine-grained understanding capability. Initially, when the model is incapable of distinguishing between the *hard negatives* and true pairs, the threshold ought to be set low. As the training progresses and the model’s fine-grained understanding improves, it should assign a larger disparity in scores between the *hard negatives* and true pairs. This optimization process can be seen as an instance of curriculum learning, where a gradually increasing threshold is expected to improve convergence, reduce overfitting, and enhance generalization[32]. In this context, the threshold reflects both the task’s complexity and the model’s capability. Therefore, at training step t , the threshold for a specific type $\{k | k \in (rel, att, act, obj)\}$ is calculated as follows:

$$Th_k^t = \frac{1}{|\mathcal{B}|} \sum_{(I,T) \in \mathcal{B}} (S^{t-1}(I, T) - S^{t-1}(I, T_k)) \quad (5)$$

And the final Cross-modal Rank with adaptive threshold loss at step t is:

$$\mathcal{L}_{cmr} = \sum_{(I,T) \in \mathcal{B}} \sum_{T_k \in \mathcal{T}_{hn}} \max(0, S(I, T_k) - S(I, T) + Th_k^t) \tag{6}$$

Our empirical observations suggest that without a constraint on the threshold, the value for relation hard negatives (*hard negatives*) tends to increase too quickly, impeding the training process. This phenomenon arises because unlike other hard negatives, these are not created by replacing original words with plausible alternatives, resulting in possibly implausible sentences that the model can easily distinguish from true pairs. This leads to a significant disparity in similarity scores. To ensure stable training, it's thus essential to impose an upper bound u on the threshold:

$$Th_k^t = \min \left(u, \frac{1}{N} \sum_{(I,T) \in \mathcal{B}} (S^{t-1}(I, T) - S^{t-1}(I, T_k)) \right) \tag{7}$$

Subsequently, incorporating the loss weight hyper-parameters α and β , the final loss function can be expressed as follows:

$$\mathcal{L} = \mathcal{L}_{itc(hn)} + \alpha \cdot \mathcal{L}_{imc} + \beta \cdot \mathcal{L}_{cmr} \tag{8}$$

4 Experiments & Results

4.1 Setup

Model In our study, we conduct experiments utilizing two distinct models. The first is the CLIP, which serves as a foundational model in the vision-language domain. The CLIP has been widely adopted due to its representative nature and the efficacy of its associated training loss function. In addition to CLIP, we also perform experiments with the X-VLM. X-VLM is a robust, fine-grained model that has achieved state-of-the-art performance on a multitude of fine-grained benchmarks [2].

The selection of these two representative models for our experiments is intended to demonstrate the broad applicability of our proposed method. By examining the results obtained from both models, we can better understand the potential implications and utility of our approach across the VLM spectrum.

Datasets All models are trained using the MSCOCO dataset following previous work[34]. It is then evaluated against fine-grained benchmarks including ARO[34], VL-CheckList[36],

and VALSE[21] (see Tab 1 for an overview of dataset statistics). However, benchmarks that are not publicly released, like COCO/Flickr30k from ARO, are deliberately not included in our evaluation. Although Winoground is designed for compositionality which is one type of fine-grained ability, Diwan et al.[3] showed that it has many other challenges such as commonsense reasoning and unusual image/text understanding. Our objectives are not designed to cater to these challenges, hence we do not consider Winoground to be a suitable evaluation benchmark for the scope of this work. The evaluation in all selected benchmarks involves the comparison of a positive caption against a negative one for a given image. This binary choice implies that the probability of random success is 50%, and each example scores either 1 or 0. All evaluations are conducted in a zero-shot manner.

Benchmark	Task	# image-text pairs
<i>Fine-grained Tasks</i>		
ARO	Relation, Attributes	24k
VALSE	Linguistic Phenomena	6.8k
VL-CheckList	Objects, Attributes and Relations	410k

Table 1: Overview of benchmarks.

Implementation Details For CLIP fine-tuning we use ViT/32-B model and training codebase from Open-CLIP, for X-VLM we follow the original code repository and choose X-VLM-16M. In most experiments, unless stated otherwise, we fine-tune models for five epochs on 2 A100 GPUs, with a total batch-size of 256 for CLIP and 64 for X-VLM. The training parameters are set as default. We perform hyper-parameters search for α, β for the CLIP model on COCO validation split with our generated hard negatives, and pick hyper-parameters that yield the highest Recall@1 for text retrieval. We find $\alpha = 0.2, \beta = 0.2$ yield the best results at epoch 5, and use the same α, β and training epoch for X-VLM fine-tuning. We choose several strong baselines for comparison: (1) OpenAI's

Model	ARO					VALSE				
	Relation	Attribution	Existence	Plurality	Counting	Relations	Actions	Coreference	Foil-it	Avg
Random	50									
BLIP	59.0	88.0	86.3	73.2	68.1	71.5	69.1	51.0	93.8	69.96
LXMERT†	-	-	78.6	64.4	58.0	60.2	50.3	45.5	87.1	59.6
CLIP	59.3	62.9	68.7	57.1	61.0	65.4	74.8	52.5	89.8	65.3
NegCLIP	80.2	70.5	76.8	71.7	65.0	72.9	83.2	56.2	91.9	71.6
CLIP <i>Ours</i>	83.0	76.4	78.6	77.7	64.4	74.4	84.9	54.7	93.7	72.5
XVLM-coco	73.4	86.8	83.0	75.6	67.5	69.8	71.2	48.0	94.8	69.5
XVLM <i>Ours</i>	73.9	89.3	83.3	73.8	69.8	70.0	71.5	48.4	93.3	70.8

Table 2: **Results (%) of ARO and VALSE.** The best scores for each section are highlighted in bold. † represents scores are extracted from papers.

Model	VL-CheckList									
	Attribute					Object		Relation		Avg
	Action	Color	Material	Size	State	Location	Size	Action	Spatial	
Random Chance	50									
BLIP†	79.5	83.2	84.7	59.8	68.8	83.0	81.3	81.5	59.5	75.7
CLIP-SVLC†	69.4	77.5	77.4	73.4	62.3	-	-	74.7	63.2	-
CLIP	70.5	69.4	69.5	60.7	67	80.2	79.7	72.2	53.8	69.2
NegCLIP	72.1	75.7	78.1	61.3	67.3	84.4	83.8	80.7	57.1	73.4
CLIP <i>Ours</i>	75.6	72.7	79.7	65.3	69.8	84.8	84.5	78.5	65.0	75.1
XVLM-coco	80.4	81.1	83.1	60.3	70.8	86.3	85.3	79.0	61.8	76.5
XVLM <i>Ours</i>	80.5	76.0	80.6	67.2	69.8	87.3	86.6	80.8	78.6	78.6

Table 3: **Results (%) of VL-CheckList.** The best scores for each section are highlighted in bold. † represents scores are extracted from papers.

pre-trained CLIP[23], (2) BLIP[14], (3) LXMERT[28], (4) NegCLIP[34] - the former state-of-the-art, (5) X-VLM-coco[35] - currently the most effective model for fine-grained understanding which is finetuned on MSCOCO, and (6) CLIP-SVLC[4] which also incorporates hard negatives but trained on larger CC3M.

4.2 Enhancement on compositional understanding

Results from the ARO and VALSE benchmarks are presented in Tab 2. On the ARO benchmark, when we apply our approach, we see improvement for both models for the Relation and Attribution splits. Our method, when applied to CLIP, provides a substantial enhancement over the baseline CLIP, surpassing the previous state-of-the-art, NegCLIP, by a wide margin: 2.8% in Relation and 5.9% in Attribution. With respect to X-VLM, our method led to a 2.5% improvement in Attribution category and a modest 0.5% improvement in Relation category. On the VALSE benchmark, our approach, when implemented on CLIP, improves performance across all splits compared to the baseline CLIP and outperforms NegCLIP in 5 out of 7 categories, with a macro-average (equitably averages performance across classes) improvement of 0.9%. When applied to X-VLM, we observe an improvement in 5 out of 7 categories compared to the baseline, though performance declines in two categories. The macro-average improvement is 1.3%. Results on VL-CheckList is shown in Tab 3. Our losses, when integrated with CLIP, yield substantial enhancements over the baseline, outperforming NegCLIP in seven out of nine subcategories. This translates into an average gain of 6.9% over the baseline and a 1.7% improvement compared to NegCLIP. While our losses applied to X-VLM exhibit improvement in some areas, it also shows declines in others, yielding an average improvement of 2.1%. Detailed results on each sub-categories are included in the supplementary materials.

Overall, our methods enhance the performance of both CLIP and X-VLM models in the *Existence*, *Relations*, and *Actions* categories across three datasets, likely due to our generation of relation-swap, verb-swap, and noun-swap hard negatives. However, in certain categories, our method’s effectiveness varies between CLIP and X-VLM due to differences in their architecture and training

losses. Interestingly, for some categories, such as ARO-Relation, VALSE-Relation etc., X-VLM with our proposed objectives does not surpass CLIP with our proposed objectives. We hypothesize this might be because the hyperparameters may not be optimal for X-VLM. Due to computing constraints, we could not tune hyperparameters separately for X-VLM, and apply the same from CLIP finetuning.

Model	ARO					VALSE				
	Relation	Attribution	Existence	Plurality	Counting	Relations	Actions	Coreference	Foil-it	Avg
CLIP	59.3	62.9	68.7	57.1	61.0	65.4	74.8	52.5	89.8	65.3
NegCLIP	80.2	70.5	76.8	71.7	65.0	72.9	83.2	56.2	91.9	71.6
<i>itc</i>	61.5	65.8	76.8	72.0	64.4	65.2	73.4	59.4	90.3	69.4
<i>itc(hn)</i>	79.3	70.3	83.2	74.4	62.8	72.3	81.1	56.6	93.6	71.6
<i>itc(hn)+imc</i>	81.9	74.5	79.8	77.6	66.5	76.3	85.3	56.2	93.5	73.5
<i>itc(hn)+cmr</i>	80.5	71.4	83.0	75.3	64.8	75.0	84.2	52.5	94.0	72.3
<i>itc(hn)+cmr+imc</i>	83.0	76.4	78.6	77.7	64.4	74.4	84.9	54.7	93.7	72.5

Table 4: **Results (%) of ARO and VALSE on CLIP with ablations.** The best scores for each section are highlighted in bold.

Model	VL-CheckList									Avg
	Attribute					Object		Relation		
	Action	Color	Material	Size	State	Location	Size	Action	Spatial	
CLIP	70.5	69.4	69.5	60.7	67	80.2	79.7	72.2	53.8	69.2
NegCLIP	72.1	75.7	78.1	61.3	67.3	84.4	83.8	80.7	57.1	73.4
<i>itc</i>	73.4	75.8	74.8	61.6	64.8	83.8	83.1	74.5	45.3	70.7
<i>itc(hn)</i>	77.6	82.0	82.1	62.1	68.0	86.1	85.3	79.9	61.2	76.0
<i>itc(hn)+imc</i>	75.0	72.0	78.6	64.8	68.8	84.7	84.3	78.1	62.8	74.3
<i>itc(hn)+cmr</i>	76.4	82.5	84.2	62.7	68.7	85.7	85.0	80.4	66.3	76.9
<i>itc(hn)+imc+cmr</i>	75.6	72.7	79.7	65.3	69.8	84.8	84.5	78.5	65.0	75.1

Table 5: **Results (%) of VL-CheckList on CLIP with ablations .** The best scores for each section are highlighted in bold.

4.3 Ablation Studies

Losses We conduct several ablation studies on the CLIP model to evaluate the effectiveness of each component of our proposed method, shown in Tab 4 and Tab 5. We observed significant performance improvements when incorporating hard negatives, underscoring their role in contrastive learning. Each individual loss proposed in our method further enhanced the performance across all benchmarks, verifying the efficacy of our approach with hard negatives.

Cumulative improvement was noted in the ARO benchmark, with the highest performance achieved using the combined loss. This trend was not mirrored in the VALSE and VL-CheckList benchmarks, where the peak performance was achieved using *itc(hn)+imc* and *itc(hn)+cmr* respectively. This divergence might be attributed to the difference in distribution between the fine-tuning (COCO) and evaluation datasets and the fact that the wide range of subcategories in VALSE and VL-CheckList may not be fully covered by the generated hard negatives, leading to varying loss behaviors. Nevertheless, our approach consistently surpassed NegCLIP in all scenarios, with the combined loss still producing commendable results.

Threshold To evaluate the effectiveness of our adaptive thresholds, we performed an ablation study on the threshold value. The adaptability feature inherently incorporates curriculum learning and provides satisfactory results without the need for an exhaustive hyper-parameter search. On the contrary, with four thresholds in our model, if we attempt n different values for each threshold, searching for fixed-threshold values necessitates an impractical n^4 trials. Consequently, we utilized a uniform fixed threshold for all hard negatives and conducted ablations on this solitary value.

Fig 4 (Top Left) demonstrates that adaptive threshold consistently outperforms the fixed one across both datasets. Fig 4 (Top Right) shows performance with different values of the upper bound (see Eq. 7) which aim to constrain the largest value attainable by *Threshold Relation*. We obtain the best results with upper bound of 10.

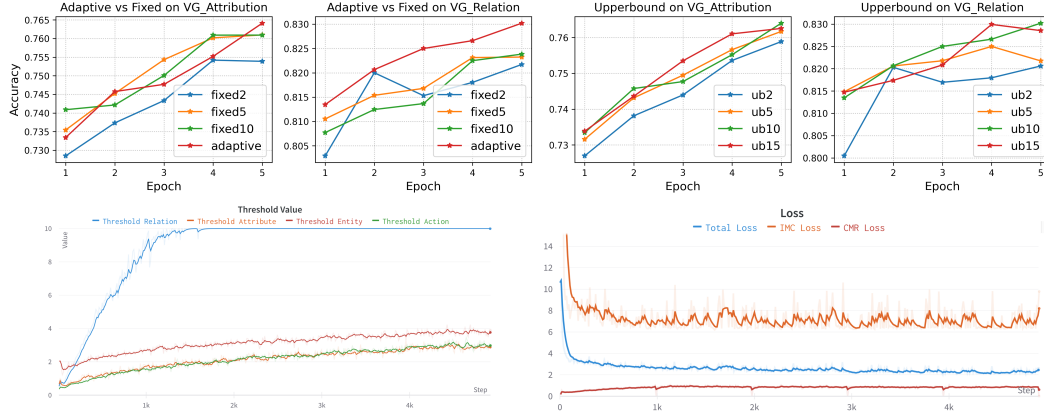


Figure 4: **Ablation study and analysis on threshold** (Top Left) Adaptive threshold vs Fixed threshold; (Top Right) Performance with different upper bound values.; (Bottom Left) Evolution of thresholds over time ; (Bottom Right) Evolution of losses over time showing stabilization of the CMR loss after initial training steps.

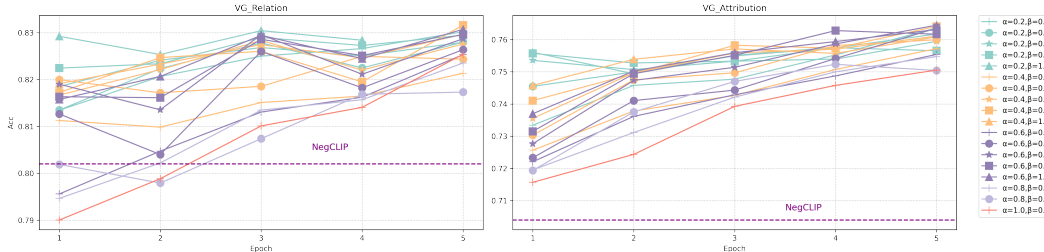


Figure 5: **Ablations of α, β on ARO.** Curves with identical values of α share the same color, while those with identical β values use the same marker.

The adaptive threshold value curve (Fig 4, Bottom Left) shows a sharp increase for *Threshold Relation* value, primarily because the relation-swap hard negatives can generate sentences with semantic and grammatical errors (e.g., sentences in Fig 3). This enables the model to easily distinguish between authentic and hard negative captions. Accordingly, our approach increases the task’s complexity by elevating the threshold, thereby providing a stronger supervisory signal to the model, forcing it to identify a larger difference between these captions.

The threshold value, calculated as the average difference between true and hard negative similarity scores, reflects both the task’s complexity in terms of the loss function and the model’s ability to discern specific types of hard negatives. The loss curve (Fig 4, Bottom Right) shows that the CMR loss stabilizes after the initial stages, indicating a balance between increasing task difficulty and the model’s adaptive capacity. This dynamic further underscores the curriculum learning aspect inherent in our adaptive threshold proposition.

Loss Weight As shown in Fig 4 (Bottom Right), the scale of CMR loss and IMC loss diverges significantly. Therefore, the selection of appropriate weight parameters is essential for successful training. Fig 5 presents ablations on α and β . Our approach exhibits robustness to variations in these hyperparameters, outperforming NegCLIP after 5 epochs on both datasets across a range of α and β values.

4.4 Standard Retrieval

We conducted standard cross-modal retrieval experiments on the COCO dataset, with the results presented in Tab 6. It was observed that our approach enhanced image retrieval performance, however, it did not bring a similar improvement to text retrieval. An observation from our study is the consistent

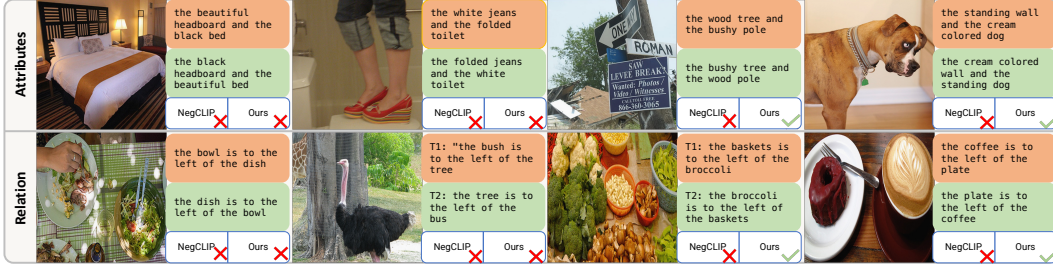


Figure 6: Some qualitative examples on ARO. Caption in red box is unmatched and in green box is matched. tick represents model predicates correctly and cross means wrong.

improvement in fine-grained tasks, despite no analogous progress in standard tasks. This supports the assertion that the performance in fine-grained tasks may not be linked with those in standard retrieval tasks as also observed in [2]. Our study has unveiled a compelling observation: our proposed approach unexpectedly boosts the efficiency of text-to-image retrieval tasks, which contrasts with our original expectation of improving image-to-text performance. Notably, our technique is chiefly designed to generate hard negative captions, which in essence aids a model in distinguishing one image from various captions—a task fundamentally associated with image-to-text processing. This surprising finding necessitates further investigation.

4.5 Qualitative Examples

In Figure 6, we provide a comparison of successful and unsuccessful predictions made by our method, juxtaposed with those from NegCLIP. The failures highlight certain obstacles that impede correct predictions. These include challenges associated with visual recognition of intricate objects, such as ‘headboard’ and ‘bow’ in the first column, and a ‘toilet’ in the second column.

5 Conclusion

Detailed understanding of complex scenes is fundamental to human visual perception, yet it remains challenging for current VLMs. In our study, we introduce a featured hard negative generation strategy and two losses that infuse fine-grained supervision into pretrained VLMs using feature-derived hard negatives. Our intra-modal contrastive loss mitigates high intra-modal similarity while our cross-modal rank loss ensures a minimum distance between true and hard negative image-text pairs, with the adaptive threshold functioning as curriculum learning to enhance performance. Our method exhibits empirical superiority on the ARO, VALSE, and VL-CheckList benchmarks, surpassing previous techniques without additional annotations.

6 Limitations

While our approach has proven effective, ideally we would incorporate the proposed losses during the pretraining stage to further enhance its functionality. However, due to computational constraints, we have not been able to do so. Future work could look into integrating these losses in the pretraining phase to improve fine-grained understanding capabilities. Regarding the ablation studies, not all hyperparameters could be ablated due to compute limitations, implying that better results could potentially be obtained with different hyperparameters. Our hard negative generation is predominantly rule-based and use small language models, which can lead to semantically and syntactically incorrect sentences. A potential improvement could involve using large language models to rectify these sentences or utilizing other tools such as a scene graph parser, which we leave for future exploration.

Task	CLIP	NegCLIP	Ours
<i>fine-grained tasks</i>			
VG-Relation	59.3	80.2	83
VG-Attribution	62.9	70.5	76.4
VALSE	65.3	71.6	72.5
VL-Checklist	69.2	73.4	75.1
<i>standard retrieval tasks</i>			
COCO Image R@1	30.1	41.0	42.2
COCO Text R@1	50.0	56.0	47

Table 6: Standard retrieval Results. **Image R@1** corresponds to text-to-image retrieval and **Text R@1** corresponds to image-to-text retrieval. The fine-grained results are same as those reported in Tab 2 and 3 above, presented here again for completeness.

References

- [1] Jean-Baptiste Alayrac, Jeff Donahue, Pauline Luc, Antoine Miech, Iain Barr, Yana Hasson, Karel Lenc, Arthur Mensch, Katie Millican, Malcolm Reynolds, Roman Ring, Eliza Rutherford, Serkan Cabi, Tengda Han, Zhitao Gong, Sina Samangooei, Marianne Monteiro, Jacob Menick, Sebastian Borgeaud, Andrew Brock, Aida Nematzadeh, Sahand Sharifzadeh, Mikolaj Binkowski, Ricardo Barreira, Oriol Vinyals, Andrew Zisserman, and Karen Simonyan. Flamingo: a visual language model for few-shot learning, 2022.
- [2] Emanuele Bugliarello, Laurent Sartran, Aishwarya Agrawal, Lisa Anne Hendricks, and Aida Nematzadeh. Measuring progress in fine-grained vision-and-language understanding, 2023.
- [3] Anuj Diwan, Layne Berry, Eunsol Choi, David Harwath, and Kyle Mahowald. Why is winoground hard? investigating failures in visuolinguistic compositionality, 2022.
- [4] Sivan Doveh, Assaf Arbelle, Sivan Harary, Rameswar Panda, Roei Herzig, Eli Schwartz, Donghyun Kim, Raja Giryes, Rogerio Feris, Shimon Ullman, and Leonid Karlinsky. Teaching structured vision language concepts to vision language models, 2022.
- [5] Samir Yitzhak Gadre, Gabriel Ilharco, Alex Fang, Jonathan Hayase, Georgios Smyrnis, Thao Nguyen, Ryan Marten, Mitchell Wortsman, Dhruva Ghosh, Jieyu Zhang, Eyal Orgad, Rahim Entezari, Giannis Daras, Sarah Pratt, Vivek Ramanujan, Yonatan Bitton, Kalyani Marathe, Stephen Mussmann, Richard Vencu, Mehdi Cherti, Ranjay Krishna, Pang Wei Koh, Olga Saukh, Alexander Ratner, Shuran Song, Hannaneh Hajishirzi, Ali Farhadi, Romain Beaumont, Sewoong Oh, Alex Dimakis, Jenia Jitsev, Yair Carmon, Vaishaal Shankar, and Ludwig Schmidt. Datacomp: In search of the next generation of multimodal datasets, 2023.
- [6] Weifeng Ge, Weilin Huang, Dengke Dong, and Matthew R. Scott. Deep metric learning with hierarchical triplet loss. In *European Conference on Computer Vision*, 2018.
- [7] Yash Goyal, Tejas Khot, Douglas Summers-Stay, Dhruv Batra, and Devi Parikh. Making the v in vqa matter: Elevating the role of image understanding in visual question answering, 2017.
- [8] Ben Harwood, B. V. Kumar, G. Carneiro, Ian D. Reid, and Tom Drummond. Smart mining for deep metric learning. *2017 IEEE International Conference on Computer Vision (ICCV)*, pages 2840–2848, 2017.
- [9] Roei Herzig, Alon Mendelson, Leonid Karlinsky, Assaf Arbelle, Rogério Schmidt Feris, Trevor Darrell, and Amir Globerson. Incorporating structured representations into pretrained vision & language models using scene graphs. *ArXiv*, abs/2305.06343, 2023.
- [10] Matthew Honnibal and Ines Montani. spaCy 2: Natural language understanding with Bloom embeddings, convolutional neural networks and incremental parsing. To appear, 2017.
- [11] Chao Jia, Yinfei Yang, Ye Xia, Yi-Ting Chen, Zarana Parekh, Hieu Pham, Quoc V. Le, Yunhsuan Sung, Zhen Li, and Tom Duerig. Scaling up visual and vision-language representation learning with noisy text supervision, 2021.
- [12] Yannis Kalantidis, Mert Bulent Sariyildiz, No’e Pion, Philippe Weinzaepfel, and Diane Larlus. Hard negative mixing for contrastive learning. *ArXiv*, abs/2010.01028, 2020.
- [13] Junnan Li, Dongxu Li, Silvio Savarese, and Steven Hoi. Blip-2: Bootstrapping language-image pre-training with frozen image encoders and large language models, 2023.
- [14] Junnan Li, Dongxu Li, Caiming Xiong, and Steven Hoi. Blip: Bootstrapping language-image pre-training for unified vision-language understanding and generation, 2022.
- [15] Yinhan Liu, Myle Ott, Naman Goyal, Jingfei Du, Mandar Joshi, Danqi Chen, Omer Levy, Mike Lewis, Luke Zettlemoyer, and Veselin Stoyanov. Roberta: A robustly optimized bert pretraining approach, 2019.
- [16] Zixian Ma, Jerry Hong, Mustafa Omer Gul, Mona Gandhi, Irena Gao, and Ranjay Krishna. Crepe: Can vision-language foundation models reason compositionally? *arXiv preprint arXiv:2212.07796*, 2022.

- [17] R. Manmatha, Chaoxia Wu, Alex Smola, and Philipp Krähenbühl. Sampling matters in deep embedding learning. *2017 IEEE International Conference on Computer Vision (ICCV)*, pages 2859–2867, 2017.
- [18] Oscar Mañas, Pau Rodriguez, Saba Ahmadi, Aida Nematzadeh, Yash Goyal, and Aishwarya Agrawal. Mapl: Parameter-efficient adaptation of unimodal pre-trained models for vision-language few-shot prompting, 2023.
- [19] Roni Paiss, Ariel Ephrat, Omer Tov, Shiran Zada, Inbar Mosseri, Michal Irani, and Tali Dekel. Teaching clip to count to ten, 2023.
- [20] Rohan Pandey, Rulin Shao, Paul Pu Liang, Ruslan Salakhutdinov, and Louis-Philippe Morency. Cross-modal attention congruence regularization for vision-language relation alignment, 2022.
- [21] Letitia Parcalabescu, Michele Cafagna, Lilitta Muradjan, Anette Frank, Iacer Calixto, and Albert Gatt. VALSE: A task-independent benchmark for vision and language models centered on linguistic phenomena. In *Proceedings of the 60th Annual Meeting of the Association for Computational Linguistics (Volume 1: Long Papers)*, pages 8253–8280, Dublin, Ireland, May 2022. Association for Computational Linguistics.
- [22] Yao Qin, Chiyuan Zhang, Ting Chen, Balaji Lakshminarayanan, Alex Beutel, and Xuezhi Wang. Understanding and improving robustness of vision transformers through patch-based negative augmentation. *ArXiv*, abs/2110.07858, 2021.
- [23] Alec Radford, Jong Wook Kim, Chris Hallacy, Aditya Ramesh, Gabriel Goh, Sandhini Agarwal, Girish Sastry, Amanda Askell, Pamela Mishkin, Jack Clark, et al. Learning transferable visual models from natural language supervision. In *International conference on machine learning*, pages 8748–8763. PMLR, 2021.
- [24] Joshua Robinson, Ching-Yao Chuang, Suvrit Sra, and Stefanie Jegelka. Contrastive learning with hard negative samples. *ArXiv*, abs/2010.04592, 2020.
- [25] Christoph Schuhmann, Richard Vencu, Romain Beaumont, Robert Kaczmarczyk, Clayton Mullis, Aarush Katta, Theo Coombes, Jenia Jitsev, and Aran Komatsuzaki. Laion-400m: Open dataset of clip-filtered 400 million image-text pairs, 2021.
- [26] Amanpreet Singh, Ronghang Hu, Vedanuj Goswami, Guillaume Couairon, Wojciech Galuba, Marcus Rohrbach, and Douwe Kiela. Flava: A foundational language and vision alignment model, 2022.
- [27] Harman Singh, Pengchuan Zhang, Qifan Wang, Mengjiao Wang, Wenhan Xiong, Jingfei Du, and Yu Chen. Coarse-to-fine contrastive learning in image-text-graph space for improved vision-language compositionality. 2023.
- [28] Hao Tan and Mohit Bansal. Lxmert: Learning cross-modality encoder representations from transformers, 2019.
- [29] Tristan Thrush, Ryan Jiang, Max Bartolo, Amanpreet Singh, Adina Williams, Douwe Kiela, and Candace Ross. Winoground: Probing vision and language models for visio-linguistic compositionality. In *Proceedings of the IEEE/CVF Conference on Computer Vision and Pattern Recognition*, pages 5238–5248, 2022.
- [30] Jiang Wang, Yang song, Thomas Leung, Chuck Rosenberg, Jinbin Wang, James Philbin, Bo Chen, and Ying Wu. Learning fine-grained image similarity with deep ranking, 2014.
- [31] Tan Wang, Kevin Lin, Linjie Li, Chung-Ching Lin, Zhengyuan Yang, Hanwang Zhang, Zicheng Liu, and Lijuan Wang. Equivariant similarity for vision-language foundation models, 2023.
- [32] Xin Wang, Yudong Chen, and Wenwu Zhu. A survey on curriculum learning, 2021.
- [33] Jiahui Yu, Zirui Wang, Vijay Vasudevan, Legg Yeung, Mojtaba Seyedhosseini, and Yonghui Wu. Coca: Contrastive captioners are image-text foundation models, 2022.

- [34] Mert Yuksekgonul, Federico Bianchi, Pratyusha Kalluri, Dan Jurafsky, and James Zou. When and why vision-language models behave like bags-of-words, and what to do about it? *arXiv e-prints*, pages arXiv-2210, 2022.
- [35] Yan Zeng, Xinsong Zhang, and Hang Li. Multi-grained vision language pre-training: Aligning texts with visual concepts, 2022.
- [36] Tiancheng Zhao, Tianqi Zhang, Mingwei Zhu, Haozhan Shen, Kyusong Lee, Xiaopeng Lu, and Jianwei Yin. VI-checklist: Evaluating pre-trained vision-language models with objects, attributes and relations, 2022.

Appendix

A Detailed Results

A.1 Results on VALSE fine-grained categories

In this section, we conduct an ablation study to examine the impact of each of the two proposed loss functions when evaluated on VALSE fine-grained categories. We report the results for the CLIP model. The results are shown in Figure 7. As the training phase progresses, a decline in the model’s performance is observed across most categories, with the notable exceptions of relations and coreference hard. This observation can be attributed primarily to out-of-distribution evaluation settings. More specifically, our model is fine-tuned on the COCO dataset. Consequently, increased training tends to result in overfitting to the COCO distribution. This overfitting ultimately yields deteriorating results on the VALSE dataset due to the inherent distributional differences. On average, the *itc(hn)+imc* configuration achieves the highest performance. However, the optimal loss function varies across categories: combined losses excel in the counting hard, counting adversarial, and plurals categories, while the *itc(hn)+cmr* configuration outperforms others in the relations, foil it, and existence categories. All loss functions proposed in this study significantly improve upon the baseline (CLIP) and outperform the previous state-of-the-art model, NegCLIP.

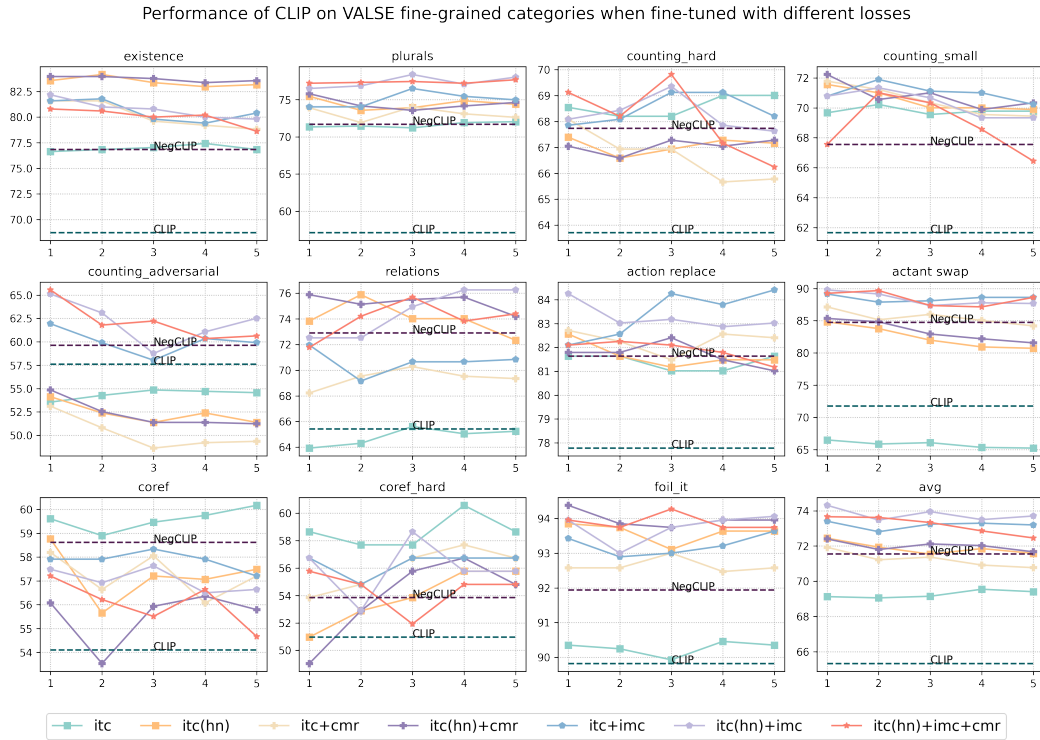


Figure 7: **CLIP Results (%) on VALSE Fine-Grained Categories.** The plots show the accuracy (represented on the y-axis) plotted against epochs (represented on the x-axis).

A.2 Fine Results on ARO

A detailed attribute wise breakdown of the performance of CLIP (fine-tuned with our proposed objectives) on the ARO Attributes dataset is shown in Table 7. Similarly, the results for ARO-relations have been presented in Table 8.

Relation	CLIP	NegCLIP	Ours	Relation	CLIP	NegCLIP	Ours
black_blue	54.76	57.14	58.33	large_cloudy	70.37	88.89	92.59
black_brown	64.76	69.52	66.67	large_gray	57.14	57.14	76.19
black_gray	51.67	71.67	55.00	large_green	64.29	82.86	82.86
black_green	67.86	70.24	77.38	large_white	70.45	78.41	88.64
black_large	70.21	55.32	65.96	large_wood	73.53	76.47	76.47
black_red	58.06	58.06	48.39	long_white	76.47	82.35	76.47
black_white	51.22	62.93	58.54	metal_brown	58.62	79.31	68.97
black_wood	50.00	69.23	65.38	metal_green	68.00	80.00	76.00
blue_black	70.59	73.53	78.43	metal_white	46.51	69.77	72.09
blue_brick	81.48	92.59	92.59	open_white	70.97	67.74	61.29
blue_brown	70.78	77.27	87.01	orange_white	62.50	65.62	62.50
blue_gray	63.83	76.60	69.15	red_black	67.65	55.88	73.53
blue_green	75.89	88.39	85.71	red_blue	72.73	81.82	88.64
blue_large	80.26	84.21	90.79	red_brown	54.76	61.90	73.81
blue_red	79.49	74.36	64.10	red_gray	37.93	68.97	75.86
blue_sitting	83.33	96.67	100	red_green	62.50	84.38	68.75
blue_standing	62.50	81.25	100	red_large	51.85	37.04	70.37
blue_tall	58.82	88.24	97.06	red_white	59.38	75.00	81.25
blue_white	71.97	84.94	82.01	silver_white	55.26	71.05	84.21
blue_wood	77.36	84.91	81.13	sitting_black	77.78	77.78	92.59
blue_young	81.82	100	100	sitting_white	60.00	64.00	76.00
brick_blue	60.00	84.00	92.00	small_brown	46.67	56.67	53.33
brown_black	61.97	63.38	77.46	small_white	61.70	70.21	63.83
brown_blue	57.14	65.87	78.57	smiling_white	74.07	81.48	96.30
brown_gray	55.56	72.22	66.67	standing_green	71.43	77.14	80.00
brown_green	60.29	80.15	79.41	striped_white	68.97	62.07	82.76
brown_large	60.00	53.33	66.67	tall_blue	79.59	95.92	91.84
brown_red	57.69	69.23	61.54	tall_green	68.97	79.31	79.31
brown_small	40.00	28.00	48.00	white_black	59.33	53.33	74.00
brown_tall	58.33	58.33	66.67	white_blue	64.08	64.08	70.39
brown_white	53.54	64.16	69.91	white_brown	60.26	57.21	71.18
brown_wood	45.45	54.55	63.64	white_clear	65.91	84.09	72.73
clear_brown	77.78	77.78	77.78	white_cloudy	53.12	62.50	59.38
clear_green	80.00	84.00	60.00	white_dark	57.89	68.42	81.58
clear_large	56.00	72.00	76.00	white_gray	38.46	44.62	45.38
clear_white	70.59	80.39	90.20	white_green	64.54	72.34	70.21
cloudy_large	80.00	100	100	white_happy	74.29	88.57	97.14
dark_white	41.18	49.02	68.63	white_large	44.58	46.99	73.49
gray_black	70.37	51.85	75.93	white_long	46.43	60.71	75.00
gray_blue	59.46	59.46	83.78	white_metal	59.38	71.88	59.38
gray_brown	67.24	65.52	77.59	white_open	51.85	59.26	81.48
gray_green	79.07	76.74	75.58	white_orange	68.00	68.00	72.00
gray_large	59.57	61.70	82.98	white_red	55.93	38.98	54.24
gray_red	68.97	58.62	86.21	white_silver	70.37	88.89	74.07
gray_white	69.57	64.35	77.39	white_sitting	67.74	77.42	90.32
gray_wood	55.32	59.57	63.83	white_small	48.48	48.48	48.48
green_black	72.41	65.52	87.93	white_smiling	78.12	87.50	100
green_blue	48.84	61.63	79.07	white_standing	70.37	66.67	81.48
green_brown	56.20	68.60	83.47	white_wood	60.00	58.57	63.57
green_gray	69.70	69.70	62.12	white_yellow	72.00	48.00	64.00
green_large	56.52	54.35	82.61	white_young	75.00	89.29	100
green_red	64.00	60.00	96.00	wood_black	58.00	86.00	86.00
green_white	65.67	70.90	80.60	wood_blue	45.28	81.13	90.57
green_wood	66.67	61.54	79.49	wood_gray	50.00	73.33	56.67
happy_white	75.00	89.29	96.43	wood_green	51.22	80.49	78.05
large_black	55.77	67.31	82.69	wood_large	46.43	60.71	92.86
large_blue	79.55	88.64	88.64	wood_white	38.69	78.10	73.72
large_brown	63.46	67.31	80.77	yellow_blue	70.59	82.35	70.59
yellow_white	57.89	71.05	50.00				

Table 7: Results(%) on each attributes.

Relation	CLIP	NegCLIP	Ours	Relation	CLIP	NegCLIP	Ours
above	47.58	59.85	64.68	on	52.32	85.57	92.16
at	58.67	93.33	98.67	on top of	42.29	75.12	84.08
behind	55.92	28.92	24.91	parked on	66.67	85.71	100
below	55.50	46.41	40.67	pulled by	66.67	33.33	11.11
beneath	80.00	70.00	40.00	pulling	33.33	100	100
carrying	33.33	83.33	83.33	reflected in	64.29	71.43	71.43
covered by	50.00	36.11	66.67	resting on	38.46	84.62	100
covered in	78.57	50.00	92.86	riding	70.59	98.04	100
covered with	56.25	56.25	87.50	sitting at	61.54	100	100
covering	39.39	57.58	66.67	sitting in	56.52	95.65	95.65
cutting	75.00	83.33	83.33	sitting on	58.86	96.57	98.29
eating	57.14	100	100	sitting on top of	50.00	90.00	90.00
feeding	90.00	80.00	80.00	standing by	66.67	91.67	91.67
grazing on	10.00	90.00	100	standing in	72.88	98.31	100
hanging on	78.57	100	92.86	standing on	59.62	100	100
holding	57.75	97.18	96.48	surrounded by	64.29	71.43	71.43
in	62.71	88.56	96.47	to the left of	49.12	50.15	51.50
in front of	53.74	75.17	79.25	to the right of	49.02	50.08	48.91
inside	50.00	91.38	86.21	under	63.64	43.18	34.09
leaning against	88.89	100	100	using	84.21	100	100
leaning on	66.67	100	100	walking in	70.00	100	100
looking at	83.87	100	96.77	walking on	78.95	100	100
lying in	46.67	100	100	watching	45.45	54.55	72.73
lying on	60.00	88.33	95.00	wearing	47.00	99.37	99.58

Table 8: Results(%) on each relations.